Structural Investigation of 3,4-Dihydroxyphenylalanine-Terminated Propanethiol Assembled on Gold

Rodrigo M. Petoral, Jr. and Kajsa Uvdal*

Laboratory of Applied Physics, Department of Physics and Measurement Technology, Linköping University, S-581 83 Linköping, Sweden

Received: March 10, 2003; In Final Form: September 2, 2003

3,4-Dihydroxyphenylalanine-terminated propanethiol (DOPA-PT), an amino acid DOPA linked to 3-mercaptopropionic acid through an amide bond, is adsorbed and self-assembled to polycrystalline gold surfaces. The structure of the adsorbates was characterized by means of X-ray photoelectron spectroscopy (XPS), infrared reflection−absorption spectroscopy (IRAS), and near-edge X-ray absorption fine structure spectroscopy (NEXAFS). Strong molecular binding of a DOPA derivative on gold surfaces through the sulfur atom was attained. Angle-dependent XPS results showed that the aromatic ring is oriented away from the gold surface. Both IRAS and NEXAFS results showed parallel orientation of the C═O bond of the amide moiety relative to the gold surface. Hydrogen bonding between amide moieties is achieved, and it seemed to provide additional orientation stabilization. Deduced orientation of the amide moiety on the short alkyl chain (or the peptide plane) is assumed to give the average orientation of the main molecular axis. The main molecular axis is estimated to have an average tilt angle of approximately 37° relative to the gold surface normal based on NEXAFS results. The aromatic ring exhibits a preferred orientation with an average tilt angle of about 64°. The experimental results showed that DOPA-thiol with amide linkage is able to self-assemble and form a layered structured film consisting of a layer of alkane chains with a gauche conformation beneath an oriented layer of DOPA.

1. Introduction

Extensive studies have been done on long-chain alkanethiols, $X(CH_2)_nSH$, where $n = 9-21$ and $X = CH_3$, OH, COOH, etc. to form well-defined self-assembled monolayers (SAMs) with different end groups to serve as model substrates for different studies.[1,2] The principal interaction in self-assembly of long chain alkanethiols on gold is the van der Waals interaction between adjacent alkyl chains in the monolayer. The interaction leads to formation of densely packed, well-ordered, and stable monolayers. Short-chain alkanethiols tend to form less stable and more disordered monolayers compared to the longer chain counterpart.[3,4] Recent studies showed that short-chain alkanethiols with amide linkages become fairly more orientationally stable.[5−7] Incorporation of amide groups in the alkanethiol chains promotes intermolecular hydrogen bonding influencing the tilt, packing density, and stability.

Amide-containing alkanethiol monolayers with a wide variety of end groups were recently studied using electrochemical, spectroscopic, and imaging techniques. Studies of amide location effects on kinetics of mediated electron transfer used scanning tunneling microscopy (STM), infrared spectroscopy, and electrochemical methods.[8] STM studies were also done to investigate the role of internal functionality in amide-containing alkanethiol molecules on Au(111).[9] Structural investigation and hydrogen-bonding effects in SAMs with amide moieties were investigated using X-ray photoelectron spectroscopy (XPS), infrared reflection−absorption spectroscopy (IRAS), and near-edge X-ray absorption fine structure spectroscopy (NEXAFS).[5−7,10] Thermal desorption studies were also employed to study the stability of laterally hydrogen bonded SAMs.[11]

Studies of SAMs generated from aromatic thiols[12−24] are significantly increasing compared to earlier days of thiol SAMs. Previous studies of phenyl-terminated SAMs, however, have been restricted to studies of those generated from simple molecules such as benzenethiol, benzyl mercaptan,[14−18] and their derivatives.[19−21] A herringbone packing of the terminal phenyl groups appears to be the thermodynamically favored structure for some of the aforementioned aromatic thiols.[15,17] It has been observed that incorporation of aromatic groups into long-chain alkanethiol SAMs plays a decisive role in the orientation of the molecules on the surface.[22] Techniques such as NEXAFS and IRAS has been employed to study the molecular orientation of the alkyl chain and phenyl ring of such long-chain alkanethiols terminated with phenyl rings.[22−23]

Immobilizing interesting biomolecules such as amino acid and peptide derivatives can be used as model surfaces for studying specific interactions with other molecules important for biomaterial and biosensor applications. In this study, we used a biomolecule, 3,4-dihydroxyphenylalanine (DOPA), linked to 3-mercaptopropionic acid through an amide bond. The said biomolecule has a big role in mussel adhesive proteins[25,26] and can as well serve as an electroactive ligand for indirect determination of aluminum in biological samples.[27] Future application of DOPA can be used as an affinity-sensing molecule for coordination of Al^{3+} existing in the body[28] and can be used to study aluminum neurotoxicity based on brain-related disease studies.[29−31]

In this work, the synthesized molecule, 3,4-dihydroxyphenylalanine-terminated propanethiol (DOPA-PT), adsorbed on gold surface through thiol chemistry is studied. Composition, chemical binding, and molecular orientation of the adsorbate are investigated by XPS, IRAS, and NEXAFS. The structure of the molecule having amide linkage in short alkyl chains with an aromatic end group is interesting to study considering its potential applications.

* Corresponding author. Fax: 46-13-288-969. E-mail: kaj@ifm.liu.se.

10.1021/jp030323s CCC: $25.00
Published on Web 11/06/2003

2. Experimental Section

2.1. Sample Preparation. The DOPA-PT was synthesized at the Department of Chemistry, Linköping University. The synthetic pathway is similar to synthesis of a tyrosine-terminated propanethiol (TPT).[32] DOPA-PT adsorbates were prepared from ethanol solutions with a concentration of 1 mM.

The gold substrates used were prepared by electron-beam evaporation of 2000 Å thick Au at a rate of 10 Å/s onto clean single-crystal Si(100) wafers. Before evaporation of the gold film, the silicon wafers were first coated with a 20−25 Å thick Ti layer at a rate of 2 Å/s. The base pressure was always $<5 \times 10^{-9}$ Torr, and the evaporation pressure was $<2 \times 10^{-8}$ Torr. The thin gold film has preferred (111) with grain size of 70−300 Å and with the outer parts of these grains showing extremely flat films.[33] The gold surfaces were cleaned in a 5:1:1 mixture of MilliQ water, 25% hydrogen peroxide, and 30% ammonia for 5 min at 80 °C and then thoroughly rinsed in MilliQ water.

The gold surfaces were incubated in the DOPA-PT solution for the duration of more than 24 h, rinsed in Milli-Q water, and then ultrasonicated in MilliQ water for 5 min. It was followed by blow drying of the surfaces with nitrogen gas, and then immediately analyzed. The DOPA-PT multilayer sample was prepared by letting a drop of high-concentration DOPA-PT dry on a prepared gold surface monolayer while letting a stream of gaseous nitrogen pass over the surface.

2.2. X-ray Photoelectron Spectroscopy. XPS was performed in a Scienta ESCA 200 spectrometer, with a base pressure of 1×10^{-10} Torr, using monochromatized Al(Kα) X-rays at $h\nu = 1486$ eV. The resolution was determined from the full width at height maximum (fwhm) of the gold Au ($4f_{7/2}$) line, which was 0.7 eV. The binding energy scale of the spectra was aligned through the Au ($4f_{7/2}$) at 84.0 eV. Angle-dependent measurements were made using photoelectron takeoff angles (TOA) of 20 and 80° with respect to the surface normal of the sample. Analysis of peak position and curve fitting is done using the ESCA Analysis software for Scienta ESCA 200.

2.3. Infrared Spectroscopy. Transmission IR measurements on DOPA-PT were made on a Bruker IFS48 Fourier transform infrared spectrometer continuously purged with N_2 gas. The samples were prepared by smearing an ample amount of the material on a CaF_2 pellet. Each spectrum is obtained by averaging 500 interferograms at 2 cm^{-1} resolution using a deuterated triglycine sulfate detector.

IRAS measurements were performed on a Bruker IFS66 Fourier transform spectrometer equipped with a grazing angle of incidence reflection accessory aligned at 85°. The infrared radiation was polarized parallel to the plane of incidence. Interferograms were apodized with a three-term Black-Harris function before Fourier transformation. The spectra were recorded by averaging 2000 interferograms at 4 cm^{-1} resolution using a liquid nitrogen cooled mercury cadmium telluride detector. The measurement chamber was continuously purged with nitrogen gas during the measurement.

2.4. Near-Edge X-ray Absorption Fine Structure Spectroscopy. The NEXAFS spectra were recorded at the synchrotron storage ring MAX II at MAX-Lab in Lund, Sweden, using the D1011 bending magnet beamline. The beamline is equipped with a modified SX-700 monochromator.[34] The measurements were carried out at the C 1s and O 1s absorption edge in the partial electron yield mode with retarding voltages of −150 and −300 V, respectively. Linear polarized synchrotron light with a polarization factor of ∼85% was used. The energy resolution was ∼0.5 eV. The incidence angle of the synchrotron light was varied from 90° (**E**-vector in surface plane) to 30° (**E**-vector near surface normal) to monitor the orientation of the DOPA-PT adsorbates. The raw NEXAFS spectra were normalized to the incident photon flux by division through a spectrum of a sputtered clean gold sample.

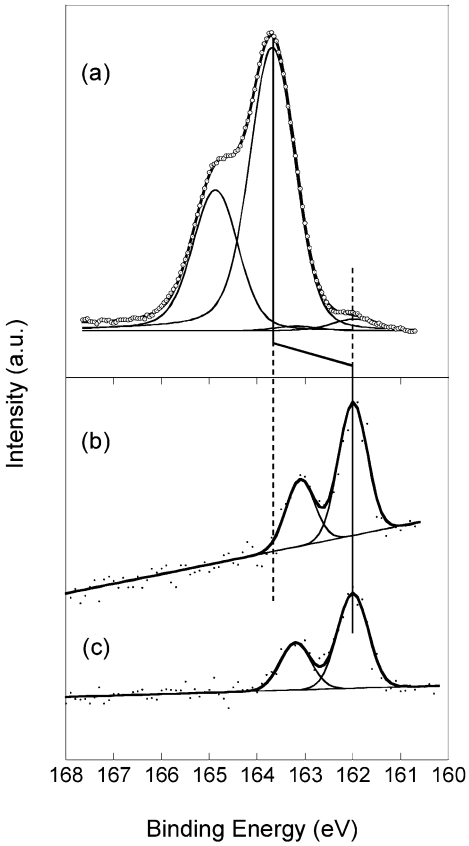

Figure 1. The S (2p) XPS core level spectra for DOPA-PT on gold: (a) thin film of the molecule (multilayer) on gold, (b) adsorbate on gold surface in bulk-sensitive mode, (c) adsorbate on gold surface in surface-sensitive mode.

3. Results and Discussion

3.1. XPS. The S (2p) and O (1s) XPS spectra for the DOPA-PT multilayer and adsorbates are shown in Figures 1 and 2, respectively. Curve fitting is done, and assignment of the best-fit curve is followed.

The sulfur peak for the DOPA-PT multilayer (Figure 1a) consists of spin−orbit split doublet with the S ($2p_{3/2}$) and S ($2p_{1/2}$) binding energies of 163.7 and 164.9 eV, respectively, with a fwhm of 1.1 eV. The peak corresponds to the unbound sulfur or the SH group.[35,36] A low-intensity shoulder on the lower energy side is correlated to the surface species. These surface species are in good agreement with the main S (2p) peaks (Figure 1b and 1c) for the DOPA-PT monolayer. The S ($2p_{3/2}$) peak for the DOPA-PT adsorbate is found at 162 eV with a fwhm of 0.6 eV. The chemical shift of 1.7 eV to lower energy compared to the multilayer is a result of a strong molecule−surface interaction. This shows that the DOPA-PT binds to the gold surface through the sulfur atoms. The sulfur binding energy of 162 eV is consistent with sulfur atoms bound to a gold surface as a thiolate species.[35−38]

In Figure 2a, three oxygen peaks are fitted in the O (1s) spectrum of the multilayer. The binding energies of the peaks, i.e., 533 and 531.2 eV, are respectively assigned to the oxygen in the hydroxyl group in the ring and oxygen in the carbonyl group of the peptide bond, consistent with the oxygen peaks of

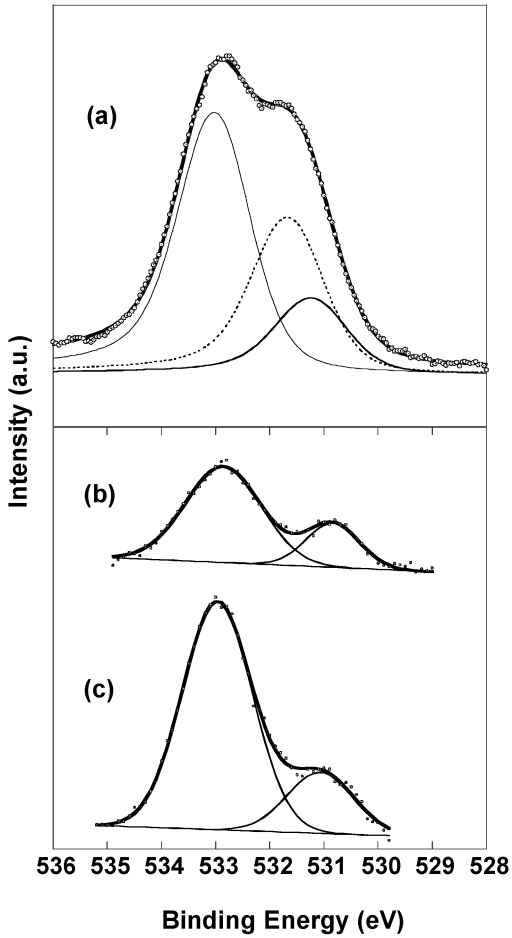

Figure 2. The O (1s) XPS core level spectra for DOPA-PT on gold: (a) thin film of the molecule (multilayer) on gold, (b) adsorbate on gold surface in bulk-sensitive mode, (c) adsorbate on gold surface in surface-sensitive mode.

TABLE 1: Relative Intensities for DOPA-Thiol/Au

	C/S	O/S	N/S	O_I/S^a	O_{II}/S^b
stoichiometric value	11	3	1	1	2
multilayer	10.4	8.7	0.7	1.3	4.6
bulk mode[c]	21.7	5.8	1.1	1.4	4.4
surface mode[d]	38.2	9.9	1.4	2	7.9

[a] O_I: oxygen peak assigned to the carbonyl group. [b] O_{II}: oxygen peak assigned to the hydroxyl groups attached to the ring. [c] TOA = 80°. [d] TOA = 20°.

a TPT monolayer[39] very similar to DOPA-PT molecule. The other peak at 531.6 eV is assigned to oxygen-related DOPA quinone, which is believed to be formed due to oxidation of L-DOPA.[25,26] The binding energy of the assigned peak is near to that of a benzoquinone and its derivatives.[40] All three fitted peaks have fwhm of 1.6 eV. For the DOPA-PT adsorbate, only two peaks are fitted with binding energies of about 533 and 531 eV with a fwhm of about 1.9 eV. The two peaks are assigned similar to the multilayer peaks appearing at the same binding energy. The oxygen species in quinone form is absent in the monolayer as compared to about 40% quinone form present in multilayer.

Results in Table 1 show the relative intensity ratios between the different elemental peaks (C (1s), N (1s), and O (1s)) to the S (2p) peak for both the multilayer and the monolayer. The relative intensity ratio between the O (1s) and S (2p) peaks (O/S) for the DOPA-PT multilayer is slightly higher than the stoichiometric value due to a relatively thinly prepared multilayer. A contribution from the surface species can still be seen in the S (2p) spectum, showing that the multilayer is quite thin.

The C/S ratio for the adsorbate is observed to be higher compared to the multilayer. The main reason for that is due to molecular orientation. The molecules are oriented with sulfur atoms close to the gold surface. A small contribution from extra hydrocarbons is to be expected due to the preparation technique of the adsorbates.

Beyond the gift of the composition of the films, XPS serves to determine the thickness of layers and yields information about the coverage and the depth of the elements. Angle-dependent XPS measurement is used to collect more detailed information about the orientation of the adsorbates. The notable increase in the C/S and O/S of the adsorbates in the surface sensitive mode as compared to the bulk mode indicates that the DOPA-PT molecules are molecularly oriented with the sulfur atoms close to the gold surface, further supporting the S−Au bond formed during adsorption. Significant increase in the relative intensity is also observed in O_{II}/S where O_{II} is the oxygen peak assigned to two OH attached to the ring. This implies that the ring is oriented far away from the sulfur atom and, consequently, far from the Au surface.

The adsorbate thickness of the DOPA-PT layer is determined by using the intensity ratio between the two different TOA of the S (2p) core level. The model and method used by Zhang et al.[41] were used to determine the thickness of the adsorbate, which is calculated to be about 13.8 Å. The calculated thickness is comparable to the average value of the thickness measured using an ellipsometer, which is 13.6 Å.

3.2. IR Results. The IR transmission (TR) and IRAS spectra of DOPA-PT are shown in parts a and b of Figure 3, respectively. The assignments of the most important peaks present on both spectra are presented in Table 2. Assignments of modes are based on related compounds found in the tables and literature.[42] The assignments are compared with the TPT molecule,[32] which is closely related to DOPA-PT.

The transmission spectrum of DOPA-PT shows all the IR-active modes of vibrations in the molecules (see Figure 3a). This spectrum serves as a reference to the IRAS spectrum (Figure 3b) of the monolayers on gold. The modes (not shown in the figure) between 2800 and 3500 cm^{-1} are assigned to amide A stretch, OH stretch, CH stretch in the aromatic ring, and the asymmetric CH_2 stretch. For the adsorbate, it is observed at the same range, too (see Table 2). The amide I, II, and III stretches are observed at 1639, 1544, and about 1255 cm^{-1}, respectively, in the transmission mode, while in IRAS, they are observed at 1654, 1552, and 1262 cm^{-1}. The bulk aromatic stretches are observed at 1602 and 1528 cm^{-1}, while the peaks at 1615 and 1530 cm^{-1} correspond to the adsorbate. The hydroxyl (OH) stretch modes in the aromatic ring are observed at 1281 and at about 1255 cm^{-1} (overlapping with amide III stretch) for the TR mode. For the RA mode, the following peaks are observed: 1295, 1279, and about 1262 cm^{-1} (overlapping with amide III stretch).

The fingerprint area, i.e., 1800−700 cm^{-1}, is complex where several vibrations that make assignments of all involved components complicated are overlapping. The region is the characteristic of the molecules to serve as their fingerprints. Significant peaks related to the peptide bond and the aromatic ring are given focus to determine the average orientation of the monoloyer on gold. Though primary peak related to amide I (C═O stretch) is obstructed with other peaks making it broad in the bulk spectrum (∼1639 cm^{-1}), a significant decrease in the intensity can be observed in the monolayer adsorbed on gold

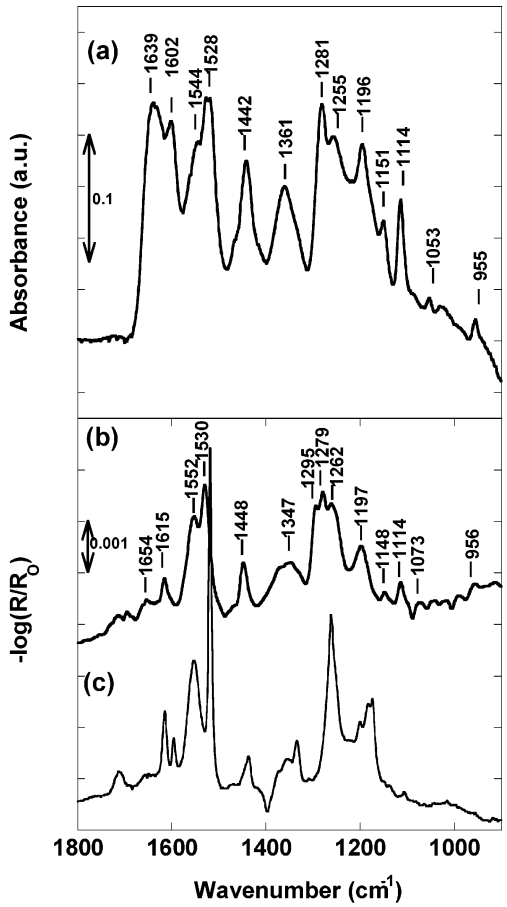

Figure 3. IR spectra of DOPA-PT and related molecule: (a) transmission spectrum of DOPA-PT dispersed on Ca_2F, (b) IRAS spectrum of DOPA-PT adsorbate on gold surface, (c) IRAS spectrum of TPT adsorbate on gold surface (see ref 32).

(~1654 cm^{-1}) when compared. Because of the surface selection rule,[43] it can be suggested that the transition dipole moment of the amide I stretch (oriented parallel to the C═O bond) is preferentially aligned almost parallel to the gold surface. Relating this to the assumption that there is a decrease in intensity of the amide A (N−H str) band appearing at 3245 cm^{-1} (not shown in the figure but relative to the peaks in the fingerprint region), which is overlapping with the OH stretches, the NH bond is assumed to be almost parallel to the surface. Interestingly enough, the amide II vibration has a slight increase in relative intensity when the molecule is adsorbed on the Au surface. Since amide II has a large contribution from NH in-plane bending, the change in the dipole moment will be in the plane and along the molecular axis that may be oriented almost perpendicular to the surface.[5] The increase in intensity is thus now consistent with the orientation of the peptide group with both the C═O and the NH bonds almost parallel to the surface. The observation is similar and consistent with previous infrared studies of alkanethiolates SAMs containing amide linkages where C═O and C−N bonds displayed preferential alignment with respect to the surface normal.[5,7,10] In addition to the deduced orientation of the peptide group, the amide II peak position of 1552 cm^{-1} is within the range of ~1550−1560 cm^{-1}, indicating hydrogen bonding between amide groups, while the non-hydrogen-bonded state would appear at ~1510 cm^{-1}.[6]

The position of a relatively stronger peak of an asymmetric CH_2 stretch provides an insight into the molecular environment of the short alkyl chains within the molecular assemblies. The location of the asymmetric CH_2 stretch peaks is a sensitive indicator of the extent of the lateral interactions between long alkyl chains according to Snyder et al.[44] Since only a small decrease in the peak frequency of monolayer compared to the bulk is observed, a relatively less-organized monolayer can be inferred. It can be interpreted that there are some regions within the monolayer where random organization can be observed. The presence of the amide linkage between short alkyl chains and the aromatic ring as a headgroup may influence the organization of the monolayers with a varying degree of organizational arrangement. Such hypothesis is in accordance to what Sabapathy et al. inferred from their observations of short-chain ferrocenylalkyl disulfides (with amide functionality) monolayers on gold.[7]

TABLE 2: IR Mode Assignments (cm^{-1}) for DOPA-Thiol in CaF_2 (Transmission, TR) and as Monolayer on Gold (Refelection−Absorption, RA) Mode[a]

tyrosine-terminated propanethiol (TPT)[b]		DOPA-thiol		
TR	RA	TR	RA	assignment
		3334	3245	amide A (NH str); O−H str
3019	3017	3030	3038	ArC−H str
2938	2978	2936	2928	CH_2 asym str
2815				
			2856	CH_2 sym str
1647	1647 (weak)	1639	1654	amide I (C═O str)
	1615	1602	1615	ArC−C str
1547	1552	1544	1552	amide II (N−C═O str)
1514	1519	1528	1530	ArC−C str
1444	1437	1442	1448	CH_2 def
1355		1361		CH_2 (?)
	1335		1347	ArC−OH ipb
		1281	1295	Ar−OH
			1279	
1240	1261	1255	1262	amide III (C−N str and N−H ipb); Ar−OH
1172	1197	1196	1197	ArC−H ipb
	1183	1151	1148	
	1174	1114	1114	
1107	1106	1053	1073	ArC−H bend
		955	956	
828	849	nd	nd	ArC−H def oop

[a] Nomenclature of mode assignment: str = stretch, asym = asymmetric, def = deformation, ipb = in plane bend, oop = out of plane, Ar = aromatic, nd = not detected. [b] Reference 32.

Peaks related to the aromatic vibrations are also assigned as seen in Table 2. The peaks related to the ring vibrations will be used to distinguish some fingerprint area to distinguish DOPA-PT from a closely related molecule, TPT.[32] Peak positions to be considered to serve as distinguishing marks between the two molecules are the Ar−OH vibration positions. TPT has only one hydroxyl group (OH) connected to the ring while DOPA-PT has two. From Figure 3b, one distinct peak can be found for TPT/Au at this region (~1261 cm^{-1}), while for DOPA-PT/Au, three emerging peaks (1295, 1279, and 1262 cm^{-1}) can be found. Though a part of this region is convoluted with the amide III peak (expected to be found at 1240 cm^{-1}), this region may help distinguish the difference between the two molecules when adsorbed on an Au surface.

3.3. NEXAFS Results. A NEXAFS spectrum reveals information about the local bonding environment around specific atoms, including the chemical states of these atoms. Determination of average orientation of the molecules can also be achieved from polarization effects observed as intensity modulations of peaks in the spectra when X-ray incidence angles are varied. The C k-edge and O k-edge spectra of DOPA-PT/Au at selected X-ray incidence angles are shown in Figures 4 and 5,

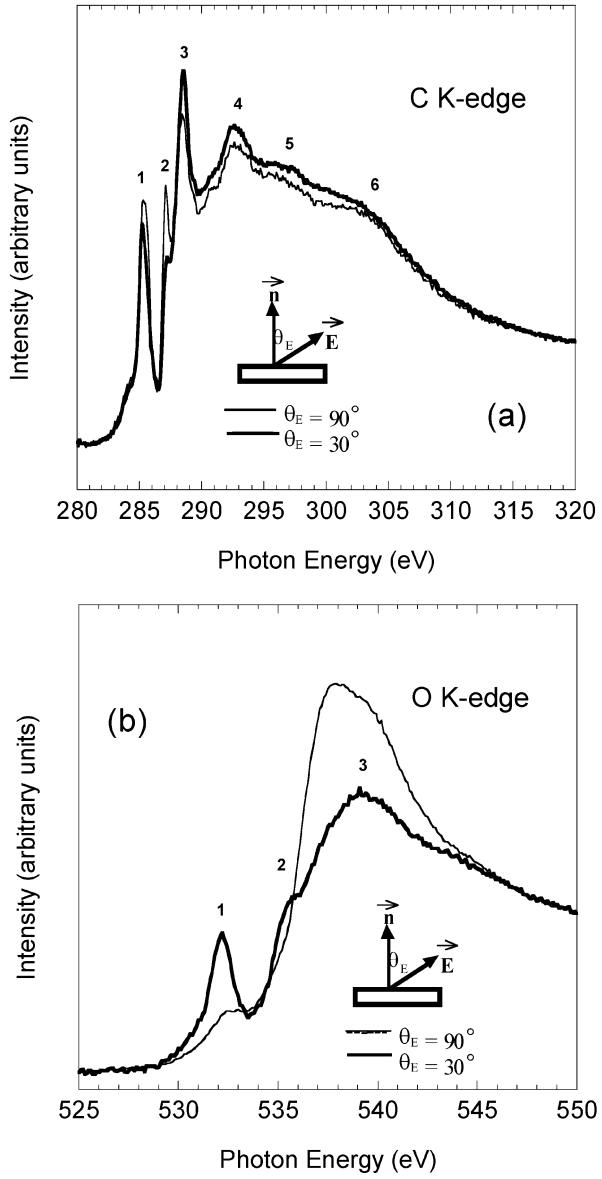

Figure 4. NEXAFS spectra of DOPA-PT on gold: (a) carbon k-edge NEXAFS spectra, (b) oxygen k-edge NEXAFS spectra.

respectively. Summaries of the assignments of the peaks are shown in Tables 3 and 4.

The C k-edge spectrum (Figure 4a) is comparable to TPT/Au reported recently.[39] Three narrow peaks associated with bound resonances can be observed. The peak at about 285 eV is associated with the $\pi^*_{C=C}$ states of the aromatic ring. If peak fitting is to be done, this peak can be split into two upon close observation consistent with phenylalanine and tyrosine amino acids identified as vibrational fine structure from the expected shifts of 1s → π^* associated with different carbon sites around the ring.[45] The second band around 287 eV is assigned as the C 1s(C−OH) → 1π^* transition. The assignment is consistent with tyrosine-related molecules[39,45,46] and is similar to that found previously for phenols[47,48] and hydroquinone.[48] The strong resonance of about 288 eV arises primarily from the C 1s → π^* transition in the carbonyl group present in the peptide bond. The peak position is consistent with the carbonyl C 1s → $\pi^*_{C=O}$ transition found for other molecular systems as nylon with amide motif,[49] disulfide containing amide,[50] and a cysteine-containing peptide tether.[51] Also at this energy, additional π^* states in the phenyl ring and Rydberg resonances in the alkyl chain carbon atoms of the molecule contribute to the intensity.[52] Broad peaks related to shape resonances at about 293 eV show an excitation of C 1s electrons into σ^*(C−C) orbitals in the ring and short alkyl chain.[23] The peak at about 296 eV is also accounted to C−C σ^* convoluted with C−N σ^*. The broad peak at about 303 eV corresponds to C═C σ^* convoluted with C═O σ^* resonances.

Difference in the intensity (intensity redistribution) of the peaks between TPT and DOPA-PT when compared is caused by hydroxyl-group substitution producing an apparent reduction in the intensity of the lines near 285 eV relative to the intensity

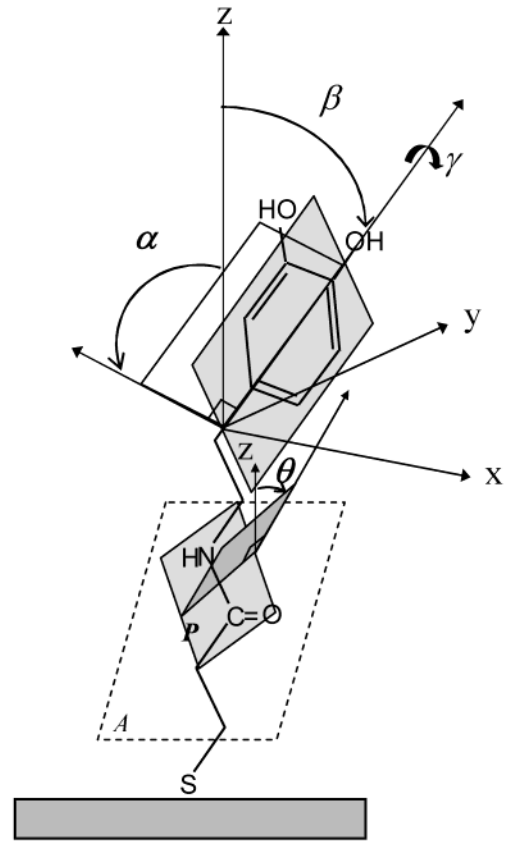

Figure 5. Schematic structure of DOPA-PT when adsorbed on gold showing angles extracted from NEXAFS (and possible angles accessible from IRAS data) used to characterize the monolayer's orientation. The peptide plane (plane P) is assumed to be in plane with the main molecular axis plane (plane A).

TABLE 3: Excitation Energies and Assignment in C k-Edge NEXAFS Spectrum of DOPA-PT/Au

peak number[a]	excitation energy (eV)	assignment
1	285.2	$\pi^*_{C=C}$
2	287.2	$\pi^*_{C=C}$ (C^b 1s → π^*)
3	288.4	$\pi^*_{C=O}$
4, 5	292.6, 296.3	σ^*_{C-C}; (σ^*_{C-N})
6	302	$\sigma^*_{C=C}$; ($\sigma^*_{C=O}$)

[a] Refer to Figure 4a. [b] C connected to OH.

TABLE 4: Excitation Energies and Assignment in O k-Edge NEXAFS Spectrum of DOPA-PT/Au

peak number[a]	excitation energy (eV)	assignment
1	532	$\pi^*_{C=O}$
2	535	O 1s → π^*; σ^*_{O-H}
3	540	σ^*_{C-O}

[a] Refer to Figure 4b.

of the carbonyl peak at 288 eV. The same observation is seen also between phenylalanine and tyrosine spectra reported recently.[45] Increase in the intensity (or more pronounced peak) of C 1s → σ^*_{C-C} around 290 eV is also observed on DOPA-PT (compared to TPT) due to −OH substitution. Additional observation of the DOPA-PT spectrum includes a weak feature at about 284 eV that could be some small amount of contaminants.

The O k-edge spectrum in Figure 4b has prominent peaks at about 532 and 540 eV. The prior peak is assigned to the O 1s → $\pi^*_{C=O}$ transition in the carbonyl part of the peptide bond. The peak position is consistent with that of the spectrum of nylon having an amide moiety.[49] The broad 540-eV peak is assigned to the σ^*(C−O), consistent with that of the phenol and hydroquinone NEXAFS spectra.[48] A small shoulder peak is observed at about 535 eV, seen more in the spectrum acquired at a grazing incidence angle. This emerging peak is seen in the O 1s spectra of alcohols[53] and was previously attributed to O 1s → σ^*_{O-H} transitions. It is also expected for O 1s → π^* transitions to contribute to this feature based on extended Huckle (EHMO) calculation results done by Francis and Hitchcock for phenols and hydroquinones.[48]

By comparison of the NEXAFS spectra acquired at X-ray incidence angles of 90° and 30°, orientation of the molecules can be predicted based on the dependence of the intensity of the angle of light incidence. The intensity of NEXAFS resonance depends on the orientation of the polarization of light with respect to the molecular orbital that is probed.[54] The intensity is maximum if the direction of the electric field of radiation (**E**-vector) and the final-state orbital are parallel with each other. Conversely, when the **E**-vector is orthogonal to the direction of the final-state orbital, the resonance is greatly attenuated. In the C k-edge spectrum for DOPA-PT adsorbate, the aromatic π^* feature is slightly more intense at normal incidence than in grazing. The band associated with the 1s → π^* excitation at C atom bound to OH groups is also more intense from normal to grazing incidence. Bands assigned to the C−C σ^* and C═C σ^* features are faintly more intense at grazing angle. This indicates that the molecules (particularly the aromatic molecules) on the average are oriented more "standing up" than "lying down". The increase in intensity of the band assigned to the C−O σ^*, which is associated with the two hydoxyl groups attached to the ring, supports more the "standing up" orientation of the aromatic ring. The band at about 288 eV associated with primarily the C═O π^* feature is more intense at the grazing incidence than the normal incidence. This indicates that the peptide is positioned with the carbonyl groups almost parallel to the gold surface. This orientation is supported further by the increase in the intensity of the band assigned to the O 1s → $\pi^*_{C=O}$ transition (see Figure 4b) at grazing incidence.

The average tilt values of the molecule are obtained by quantitative analysis of the angular dependence of the NEXAFS resonance intensities. The calculations are based on the procedure developed by Stöhr.[54] This involves taking the area of the peak at normal and grazing photon incidence and calculating the relative ratio of the integrated intensity, I_{90}/I_{30}, where I_{90} is the intensity (area) of the π^* peak at normal photon incidence and I_{30} is that at grazing incidence. The value is obtained from the function I_{90}/I_{30} versus the angle for a vector type orbitals.[54] From the small angular variation of the C═C 1π^* intensity in the spectra, it is estimated that the ring plane of the aromatic ring exhibits a preferential orientation with an average tilt angle of about 64 ± 2°. This is very close to the approximation done by Lee et al.[24] for tilt angle of phenyl-terminated SAMs having an even number of methylene units. The average tilt angle is close to the magic angle (55°) but larger than it, implying that it has a minimal degree of orientational disorder. The dichroism of the resonances associated with the $\pi^*_{C=C}$ states of the aromatic ring is rather small compared with dichroism of the π^* resonances for the thiol-derived aromatic SAMs on gold having average tilt angles of the aromatic chain of about 22°.[55] From Figure 5, the orientation of the aromatic moiety is determined by the angles α and β, which can be accessed from NEXAFS and IRAS data. The two angles can be related to the twist angle γ according to the equation[56]

$$\cos \alpha = \sin \beta \cos \gamma$$

Angle α is determined to be about 64 ± 2° while angle β is hard to determine from the IRAS spectrum due to the fact that intensities of the bands involved in calculating this angle overlap with other bands, making the peak broad in nature. Consequently, it is hard to approximate the twist angle, γ, from the aforementioned reasons. Also from the observed angular variation of intensity in the C k-edge NEXAFS spectrum, the tilt angle of the π^* orbital of C═O (in the peptide bond) is approximately 53 ± 2° relative to the normal of the surface. This angle, i.e., θ, is used to approximate the orientation of the main molecular axis. The C═O π^* orbital is perpendicular to the peptide (bond) plane, and the plane is assumed to be coplanar with the molecular axis of the molecule (see Figure 5). Also, its is assumed that the amide has a trans conformation with adjacent CH chains. From the aforementioned fact and assumption, the main molecular axis of the molecule is estimated to be tilting about 37 ± 2° relative to the surface normal. The estimated orientation of the molecule using NEXAFS analysis is very close to that of the orientation of TPT on gold.[39] For comparison, it can be mentioned that for phenyl-terminated organic surfaces,[23] a 46° tilt angle of the methylene chain with respect to the surface normal has been reported.[23]

4. Conclusion

The structure of a DOPA-derived thiol self-assembled on a gold surface was investigated using XPS, IRAS, and NEXAFS. The strength of molecule−surface interaction was investigated by XPS. Strong molecular binding of DOPA-PT on gold through the sulfur atom was attained. Angle-dependent XPS further supports the molecular orientation of sulfur atoms close to the gold surface. The aromatic ring is found to be oriented away from the gold surface. Both IRAS and NEXAFS measurements clearly show that the C═O bond in the amide moiety is oriented almost parallel to the gold surface. Orientation of the amide moiety on short alkyl chain (or the peptide plane) is assumed to give the average orientation of the main molecular axis. It shows from NEXAFS results that the main molecular axis is tilted approximately 37° relative to the gold surface normal. Results also show that the aromatic ring exhibits a preferred orientation with an average tilt angle of about 64°.

The interchain hydrogen bonding of the amide moiety present on short alkyl chains of the monolayer seemed to provide additional stabilization. The organizational behavior of these short chains, however, may be diverse and more complex compared to long-chain alkanethiols. The resulting structure of the film is an ordered layer of aromatic moieties on top of a disordered layer of hydrocarbon chains which serve as a link to the gold substrate. Formation of hydrogen bonds may overcome and lessen the inherent instability and disorderliness within monolayers with nonfunctionalized and short alkyl chains.

Acknowledgment. This project was supported by grants from The Swedish Research Council (Vetenskaprådet) and Carl Tryggers Foundation. We also wish to thank J. Ekeroth for kindly synthesizing the DOPA-PT molecule used in this study and Prof. W. Salaneck for the use of the Scienta ESCA 200 instrument. The MAX laboratory staff is also acknowledged for all their help and support during the measurements.

References and Notes

(1) Ulman, A. *An Introduction to Ultrathin Organic Films*; Academic Press: San Diego, 1991.
(2) Ulman A. *Chem. Rev.* **1996**, *96*, 1533.
(3) Nuzzo, R. G.; Dubois, L. H.; Allara, D. L. *J. Am. Chem. Soc.* **1990**, *112*, 558.
(4) Bain, C. D.; Troughton, E. B.; Tao, Y. T.; Evall, J.; Whitesides, G. M.; Nuzzo, R. G. *J. Am. Chem. Soc.* **1989**, *111*, 321.
(5) Lenk, T. J.; Hallmark, V. M.; Hoffmann, C. L.; Rabolt, J. F.; Castner, D. G.; Erdelen, C.; Ringsdorf, H. *Langmuir* **1994**, *10*, 4610.
(6) Tam-Chang, S. W.; Biebuyck, H. A.; Whitesides, G. M.; Jeon, N.; Nuzzo, R. G. *Langmuir* **1995**, *11*, 4371.
(7) Sabapathy, R. C.; Bhattacharyya, S.; Leavy, M. C.; Cleland, W. E.; Hussey, C. L. *Langmuir* **1998**, *14*, 124.
(8) Sek, S.; Palys, B.; Bilewicz, R. *J. Phys. Chem. B* **2002**, *106*, 5907.
(9) Lewis, P. A.; Smith, R. K.; Kelly, K. F.; Bumm, L. A.; Reed, S. M.; Clegg, R. S.; Gunderson, J. D.; Hutchison, J. E.; Weiss, P. S. *J. Phys. Chem. B* **2001**, *105*, 10630.
(10) Clegg, R. S.; Hutchison, J. E. *Langmuir* **1996**, *12*, 5239.
(11) Valiokas, R.; Ostblom, M.; Svedhem, S.; Svensson, S. C. T.; Liedberg, B. *J. Phys. Chem. B* **2002**, *106*, 10401.
(12) Jin, Q.; Rodriguez, J. A.; Li, C. Z.; Darici, Y.; Tao, N. J. *Surf. Sci.* **1999** *425*, 101.
(13) Duan, L.; Garrett, S. J. *J. Phys. Chem. B* **2001**, *105*, 9812.
(14) Sabatani, E.; Cohen, B. J.; Bruening, M.; Rubinstein, I. *Langmuir* **1993**, *9*, 2974.
(15) Tao, Y.-T.; Wu, C.-C.; Eu, J.-Y.; Lin, W.-L.; Wu, K.-C.; Chen, C.-H. *Langmuir* **1997**, *13*, 4018.
(16) Bandyopadhyay, K.; Patil, V.; Sastry, M.; Vijayamohanan, K. *Langmuir* **1998**, *14*, 3808.
(17) Jung, H. H.; Won, Y. D.; Shin, S.; Kim, K. *Langmuir* **1999**, *15*, 1147.
(18) Ishida, T.; Mizutani, W.; Akiba, U.; Umemura, K.; Inoue, A.; Choi, N.; Fujihira, M.; Tokumotu, H. *J. Phys. Chem. B* **1999**, *103*, 1686.
(19) Gui, J. Y.; Stern, D. A.; Frank, D. G.; Lu, F.; Zapien, D. C.; Hubbard, A. T. *Langmuir* **1991**, *7*, 995.
(20) Chang, S.-C.; Chao, I.; Tao, Y.-T. *J. Am. Chem. Soc.* **1994**, *116*, 6792.
(21) Szafranski, C. A.; Tanner, W.; Laibinis, P. E.; Garrell, R. L. *Langmuir* **1998**, *14*, 3580.
(22) Buckel, F.; Effenberger, F.; Yan, C.; Golzhauser, A.; Grunze, M. *Adv. Mater.* **2000**, *12*, 901.
(23) Wacker, D.; Weiss, K.; Kazmaier, U.; Wöll, Ch. *Langmuir* **1997**, *13*, 6689.
(24) Lee, S.; Puck, A.; Graupe, M.; Colorado, R.; Shon, Y.-S.; Lee, T. R.; Perry, S. S. *Langmuir* **2001**, *17*, 7364.
(25) Yu, M.; Hwang, J.; Deming, T. J. *J. Am. Chem. Soc.* **1999**, *121*, 5825.
(26) Yu, M.; Deming, T. J. *Macromolecules* **1998**, *31*, 4739.
(27) Zhang, F.; Bi, S.; Li, H.; Chen, Y.; Dai, L. *Electroanalysis* **2001**, *13*, 1054.
(28) Martell, A. E.; Motekaitis, R. J.; Smith, R. M. *Polyhedron* **1990**, *9*, 171.
(29) Perl, D. P.; Gajdusek, D. C.; Garruto, R. M.; Yanagihara, R. T.; Gibbs, C. J. *Science* **1982**, *217*, 1053.
(30) Kawahara, M.; Muramoto, K.; Kobayashi, K.; Mori, H.; Kuroda, Y. *Biochem. Biophys. Res. Commun.* **1994**, *198*, 531.
(31) Rawls, R. *Chem. Eng. News* **1998**, *76*, 78.
(32) Uvdal, K.; Ekeroth, J.; Konradsson, P.; Liedberg, B. *J. Colloid Interface Sci.* **2003**, *260*, 361.
(33) Uvdal, K.; Bodö, P.; Liedberg, B. *J. Colloid Interface Sci.* **1992**, *149*, 162.
(34) Nyholm, R.; Svensson, S.; Nordgren, J.; Flodström, S. S. *Nucl. Instrum. Methods Phys. Res., Sect. A* **1986**, *246*, 267.
(35) Ishida, T.; Choi, N.; Mizutani, W.; Tokumoto, H.; Kojima, I.; Azehara, H.; Hokari, H.; Akiba, U.; Fujihara, M. *Langmuir* **1999**, *15*, 6799.
(36) Petoral, R. M.; Uvdal, K. *Colloids Surf. B* **2002**, *25*, 335.
(37) Wirde, M.; Gelius, U.; Nyholm, L. *Langmuir* **1999**, *15*, 6370.
(38) Castner, D. G.; Hinds, K.; Grainger, D. W. *Langmuir* **1996**, *12*, 5083.
(39) Petoral, R. M.; Uvdal, K. *J. Electron Spectrosc. Relat. Phenom.* **2003**, *128*, 159.
(40) Ohta, T.; Yamada, M.; Kuruda, H. *Bull. Chem. Soc. Jpn.* **1974**, *47*, 1158.
(41) Zhang, Q.; Huang, H.; He, H.; Chen, H.; Shao, H. Liu, Z. *Surf. Sci.* **1999**, *440*, 142.
(42) Lin-Vien, D.; Colthup, H. B.; Fateley, W. G.; Grasselli, J. G. *The Handbook of Infrared and Raman Characteristic Frequencies of Organic Molecules*; Academic Press: San Diego, CA; 1991.
(43) Francis, S. A.; Ellison, A. H. *J. Opt. Soc. Am.* **1959**, *49*, 131.
(44) Snyder, R. G.; Strauss, H. L.; Elliger, C. A. *J. Phys. Chem.* **1982**, *86*, 5145.
(45) Kaznacheyev, K.; Osanna, A.; Jacobsen, C.; Plashkevych, O.; Vahtras, O.; Ågren, H.; Carravetta, V.; Hitchcock, A. P. *J. Phys. Chem. A* **2002**, *106*, 3153.
(46) Boese, J.; Osanna, A.; Jacobsen, C.; Kirz, J. *J. Electron Spectrosc. Relat. Phenom.* **1997**, *85*, 9.
(47) Solomon, J. L.; Madix, R. J.; Stöhr, J. *Surf. Sci.* **1991**, *255*, 12.
(48) Francis, J. T.; Hitchcock, P. *J. Phys. Chem.* **1992**, *96*, 6598.
(49) Urquhart, S. G.; Ade, H. *J. Phys. Chem. B* **2002**, *106*, 8531.
(50) Vance, A. L.; Willey, T. M.; Nelson, A. J.; Van Buuren, T.; Bostedt, C.; Terminello, L. J.; Fox, G. A. *Langmuir* **2002**, *18*, 8123.
(51) Baas, T.; Gamble, L.; Hauch, K. D.; Castner, D. G.; Sasaki, T. *Langmuir* **2002**, *18*, 4898.
(52) Bagus, P. S.; Weiss, K.; Schertel, A.; Woll, C.; Braun, W.; Hellwig, C.; Jung, C. *Chem. Phys. Lett.* **1996**, *248*, 129.
(53) Ishii, I.; Hitchcock, A. P. *J. Electron Spectrosc.* **1987**, *87*, 830.
(54) Stohr, J. *NEXAFS Spectroscopy*: Springer, Berlin; 1992.
(55) Frey, S.; Stadler, V.; Heister, K.; Eck, W.; Zharnikov, M.; Grunze, M. *Langmuir* **2001**, *17*, 2408.
(56) Rong, H.-T.; Frey, S.; Yang, Y.-J.; Zharnikov, M.; Buck, M.; Wuhn, M.; Woll, C.; Helmchen, G. *Langmuir* **2001**, *17*, 1582.